26th ABCM International Congress of Mechanical Engineering
November 22-26, 2021. Florianópolis, SC, Brazil

COB-2021-0331
SOLAR-DRIVEN DRY REFORMING OF METHANE ON THE OPEN-CELL FOAM TO IMPROVE THE ENERGY STORAGE EFFICIENCY IN A THERMOCHEMICAL FLUIDIZED BED MEMBRANE REFORMER: A COMPUTER SIMULATION APPROACH

Paulo Wendel Corderceira Costa
Daniel Ribeiro Dessaune
Jornandes Dias da Silva
Polytechnic School - UPE, Laboratory of Environmental and Energetic Technology; Rua Benfica - 455, Madalena, Recife – PE, Brazil, Cep: 50750-470
paulowendel@outlook.com
drd1@poli.br
jornandesdias@poli.br

Abstract. *The hydrodynamic characterization of the solar-driven CO_2 reforming of methane through β-SiC open-cell foam in a fluidized bed configuration is performed by reacting Methane (CH_4) with carbon dioxide (CO_2). The physical-mathematical modelling is important to design and optimize the reforming methods. Usually, the reforming methods's application through β-SiC foam bed improves the heat transfer and mass transfer due to high porosity and surface area of the β-SiC foam. Fluidized Bed Membrane (FBM) Reformers can be substantially studied as a promising equipment to investigate the thermochemical conversion of CH_4 using CO_2 to produce solar hydrogen. This work has as main objective a theoretical modelling to describe the process variables of the solar-driven CO_2 reforming of methane in the FBM reformer. The FBM reformer is filled with β-SiC open-cell foam where the thermochemical conversion is carried out. The model variables describe the specific aims of work and these objectives can be identified from each equation of the developed mathematical model. The present work has been proposed to study two specific aims as (i) The effective thermal conductivity's effect of the solid phase and (ii) molar flows of chemical components. The endothermic reaction temperature's profiles are notably increased as the numeral value of the effective thermal conductivity's effect of the solid phase is rised. The solar-driven CO_2 reforming method is suggested to improve the Production Rate (PR) of H_2 regarding the PR of CO.*

Keywords *β-SiC open-cell, fluidized bed, Solar-Driven dry Reforming, Membrane Reformer*

1. INTRODUCTION

Reforming processes which make use of solar energy to drive high temperature endothermic chemical reactions are known as solar thermochemical systems. Solar catalytic reforming of carbon dioxide (CO_2) can be carried out in a Solar Fluidized Bed Membrane (SFBM) reformer as an intensification process. The intensification strategy can lead to the development and the re-design of more compact and efficient new processes that allow better exploitation of raw materials, lower energy consumption and plant volume reduction. The technology of the solar reforming process in a SFBM reformer contributes to the key innovative element of sustainable development (Villafán-Vidales et al., 2017). In dry reforming process, methane (CH_4) reacts with carbon monoxide (CO_2) in the reaction zone (shell) of the SFBM reformer to produce a product mixture of hydrogen (H_2) and carbon monoxide (CO) (Chein et al., 2017; Chen et al., 2018). Reforming reactions are highly endothermic and can be performed with active catalysts (Ni, Rh) at high temperature, high pressure and steam-carbon ratio (S/C) varying between 1.4 and 4 (Cruz and Silva, 2017).

Solar thermochemical reforming is based in the use of concentrated solar energy as a heating source of high temperature for conducting an endothermic chemical transformation. The solar reforming technology can be used to produce renewable energies (as solar hydrogen (H_2) production) as from solar thermochemical reaction systems (STRSs). The production of solar H_2 in SFBM reformer is highlighted by changing the reaction equilibrium toward the product side through effective pressure difference induced by the continuous removal of H_2 over the membrane (Jin et al., 2018; Anjos et al., 2018). The commercial separation of H_2 through metallic membranes is mainly focused on palladium alloys membrane. Pd-based membranes have been proposed for the separation of H_2 for many years due to the selectivity to hydrogen permeation (Silva and Abreu, 2016). The fabrication of Pd membranes for the separation of H_2 has increased due the need of use in the reforming processes at high temperature, and applications for the separation processes in chemical, petrochemical, and petroleum industries.

Mathematical modelling is useful to investigate the effects of key operating parameters, optimization, and scale-up. For SFBM reformers, the permeation rate's importance on the diffusion rate needs to be included to account for radial gradients because of the polarization's effect in the vicinity of the membrane (Cruz and Silva, 2017). From the point of theoretical view, the polarization exists in all membrane separation processes due to the selective permeability of membrane (Nagy, 2010). The two-dimensional mathematical models are commonly used to estimate the temperature and concentration polarization profiles of the membrane processes. For this reason, a 2D approach able to systematically take into account this phenomenon is approached in this work.

In this study, a mathematical model has been developed to investigate the heat and mass transfer phenomena coupled with thermochemical reaction kinetics in SFBM reformer module. The performance from SFBM reformer using the solar reforming process is numerically investigated in terms of the temperature profiles of the endothermic reaction. On the other hand, it was also studied the reactant and product distribution as well as conversions of CH4 and CO2 in SFBM reformer.

2. PROBLEM DESCRIPTION

The schematic setup from Figure 1 shows a solar-driven SFBM reformer module. In this setup, a solar tower and packed bed (molten-salt) are coupled to the SFBM reformer module to keep the dynamic energy storage. The first loop in the system is a closed loop of CO_2 that is heated by a solar tower and it transports the thermal energy to the fluidized bed reformer. The hot CO_2 is circled from the packed bed (molten-salt) where a portion of CO_2 come back towards the solar tower and other part is discharged into the SFBM reformer module. The inclusion of the solar tower and packed bed (molten-salt) allows for dynamic energy storage that can be used to improve the SFBM reformer module efficiency under real operating conditions. This work focuses only on the SFBM reformer module's modelling.

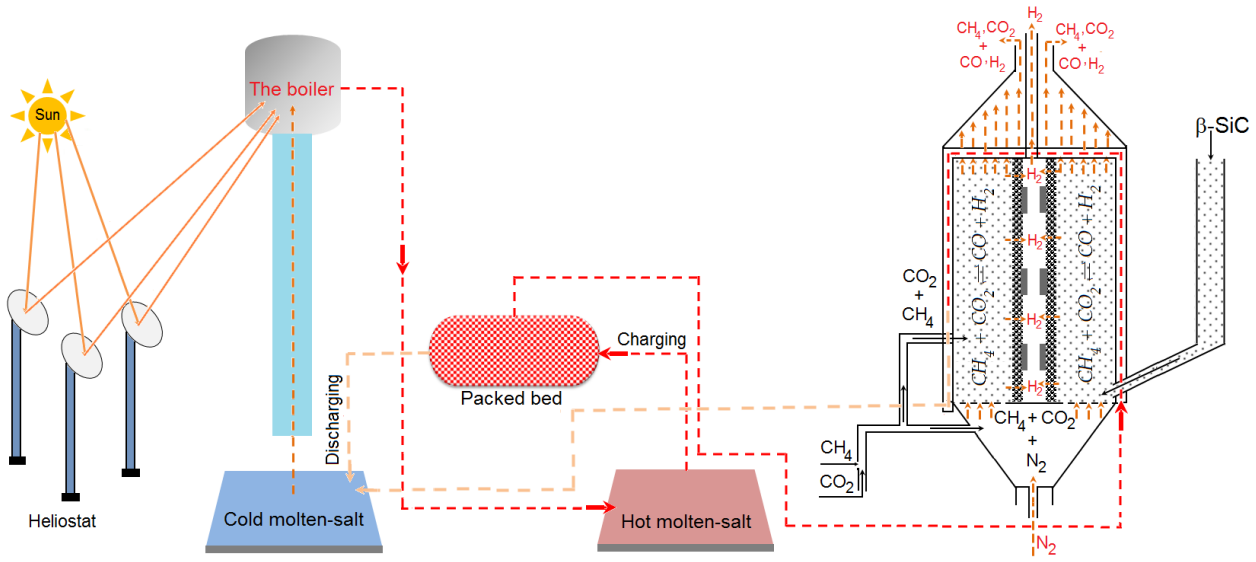

Figure 1. Schematic setup of a solar-driven SFBM reformer module.

2.1 Methodology

The schematic setup from Figure 1 is built of solar tower, packed bed (molten-salt), and SFBM reformer module, respectively. The methodology reported in this work consists of the following steps: (i) kinetic modelling of the solar reforming process of CO_2, (ii) SFBM reformer module modelling, (iii) shell side's model equations on the SFBM reformer module, (iv) permeate side's model equations on the SFBM reformer module, (v) numerical solution of model equations.

2.2 Kinetic mechanism

The reforming reaction of CO_2 is essential to produce H_2 and syngas (H_2 e CO) which are highly endothermic. The reforming process has a limited equilibrium and comprises one reforming reaction as follows.

$$CH_4 + CO_2 \rightleftharpoons 2CO + 2H_2 \; ; \; \Delta H^0_{298K} = +247\, kJ / mol \tag{1}$$

2.3 Kinetic model

The overall rate equation of the reaction, Eq. (1), is based on the Langmuir-Hinshelwood kinetic model and it can be found in Chen et al., (2018) as follows.

$$R_{CO_2} = \frac{k_{CO_2} K_{CH_4} K_{CO_2} P_{CH_4} P_{CO_2}}{\left(1 + K_{CH_4} P_{CH_4} + K_{CO_2} P_{CO_2}\right)^2} \tag{2}$$

In Eq. (2), R_{CO2} (kmol/$kg_{cat.}$h) is the kinetic rate from reforming reaction; k_{CO2} (kmol/ $kg_{cat.}$h) is the kinetic rate constant from reforming reaction, K_{CH4} is the surface adsorption equilibrium constant of CH_4, K_{CO2} (kPa^{-1}) is the surface adsorption equilibrium constant of CO_2, P_{CH4} (kPa) is the partial pressure of CH_4, P_{CO2} (kPa) is the partial pressure of CO_2, respectively.

2.4 Direct modelling of the heat and mass transfer

The gas-solid contact in the fluidized bed system improves the heat and mass transfer because of the interfacial surface's effect of solid particles. The use of mathematical models can be used to predict the heat and mass physical phenomena in the fluid-solid systems. Thus, it was developed a dynamic mathematical model that involves the SFBM reformer module's heat and mass transfer equations as follows.

2.5 Heat transfer in the shell side

An energy balance equation is developed to describe the gas temperature on the SFBM reformer module shell side. The governing energy balance of the gaseous phase is built as follows.

- Energy equation for the gaseous phase in the shell side;

$$\varepsilon_b \rho_{sh,b} C_{p,sh,b} \left(\frac{\partial T_{sh,b}}{\partial t} + u_b \frac{\partial T_{sh,b}}{\partial z} \right) = \lambda_{r,eff,b} \frac{1}{r} \frac{\partial}{\partial r} \left(r \frac{\partial T_{sh,b}}{\partial r} \right) - h_{bs} A_{bs} \left(T_{sh,b} - T_{sh,s} \right) \tag{3}$$

- Initial and boundary conditions for Equation (3) are defined as;

$$T_{sh,b}\Big|_{t=0} = T_{sh,b,0} \,;\; T_{sh,b}\Big|_{z=0^+} = T_{sh,b,in.} \,,\; \frac{\partial T_{sh,b}}{\partial z}\bigg|_{z=L} = 0 \,;\; \frac{\partial T_{sh,b}}{\partial r}\bigg|_{r=R/2} = \frac{h_{bs}}{\lambda_{r,eff,b}} \left[T_{sh,b} - \left(T_{sh,s} + \frac{T_{sh,m} + T_{p,m}}{2} \right) \right] \,,\; \frac{\partial T_{sh,b}}{\partial r}\bigg|_{r=0} = 0 \tag{4}$$

On the other hand, an energy balance equation is also built up to report the solid temperature along the SFBM reformer module shell side as follows.

- Energy equation for the solid phase in the shell side;

$$\rho_{sh,s} C_{p,sh,s} \frac{\partial T_{sh,s}}{\partial t} = \lambda_{r,eff,s} \frac{1}{r} \frac{\partial}{\partial r} \left(r \frac{\partial T_{sh,s}}{\partial r} \right) - \rho_{sh,s} C_{p,sh,s} u_s \frac{\partial T_{sh,s}}{\partial z} - h_{sg} \frac{6}{d_p} \frac{\left(1 - \varepsilon_b\right)}{\varepsilon_b} \left(T_b - T_s \right) + \rho_s \frac{\left(1 - \varepsilon_p\right)}{\varepsilon_p} \Delta H_{CO_2} \eta_{CO_2} R_{CO_2} \tag{5}$$

- Initial and boundary conditions for Equation (5) are defined as;

$$T_{sh,s}\Big|_{t=0} = T_{sh,s,0}\,;\, T_{sh,s}\Big|_{z=0^+} = T_{sh,s,in.}\,,\, \frac{\partial T_{sh,s}}{\partial z}\Big|_{z=L} = 0\,;\, \frac{\partial T_{sh,s}}{\partial r}\Big|_{r=R/2} = \frac{h_{sb}}{\lambda_{r,eff,s}}\left[T_{sh,b} - \left(T_{sh,s} + \frac{T_{sh,m}+T_{p,m}}{2}\right)\right],\, \frac{\partial T_{sh,s}}{\partial r}\Big|_{r=0} = 0 \quad (6)$$

2.6 Gaseous bubble's mass transfer in the shell side

Chemical components (i = CH_4, CO_2 and CO) are not permeated because the Pd-based membrane is built to permeate only H_2 of the shell side into the permeation side. Mass balance equations to each component on the gaseous bubble i in the SFBM reformer module's shell side are reported as follows.

- Mass balance of components i on the gaseous bubble in the shell side;

$$\frac{\partial C_{sh,b,i}}{\partial t} = D_{r,eff,b}\frac{1}{r}\frac{\partial}{\partial r}\left(r\frac{\partial C_{sh,b,i}}{\partial r}\right) - u_b\frac{\partial C_{sh,b,i}}{\partial z} + k_{bs,i}\frac{3}{R_p}\frac{\left(1-\varepsilon_b\right)}{\varepsilon_b}\left(C_{sh,b,i} - C_{sh,s,i}\right) \quad (7)$$

- Initial and boundary conditions for Equation (5) are defined as;

$$C_{sh,b,i}\Big|_{t=0} = C_{sh,b,i,0}\,;\, C_{sh,b,i}\Big|_{z=0^+} = C_{sh,b,i,in.}\,,\, \frac{\partial C_{sh,b,i}}{\partial z}\Big|_{z=L} = 0\,;\, \frac{\partial C_{sh,b,i}}{\partial r}\Big|_{r=R/2} = \frac{k_{bs}}{D_{r,eff,b}}\left(C_{sh,b,i} - C_{sh,s,i}\right),\, \frac{\partial C_{sh,b,i}}{\partial r}\Big|_{r=0} = 0 \quad (8)$$

- Mass balance of H_2 on the shell side;

$$\frac{\partial C_{sh,b,H_2}}{\partial t} = D_{r,eff,H_2}\frac{1}{r}\frac{\partial}{\partial r}\left(r\frac{\partial C_{sh,b,H_2}}{\partial r}\right) - u_b\frac{\partial C_{sh,b,H_2}}{\partial z} + k_{bs,H_2}\frac{3}{R_p}\frac{\left(1-\varepsilon_b\right)}{\varepsilon_b}\left(C_{sh,b,H_2} - C_{sh,s,H_2}\right) - \frac{\pi}{L}J_{H_2} \quad (7)$$

- Initial and boundary conditions for Equation (7) are defined as;

$$C_{sh,b,H_2}\Big|_{t=0} = C_{sh,b,H_2,0}\,;\, C_{sh,b,H_2}\Big|_{z=0^+} = C_{sh,b,H_2,in.}\,,\, \frac{\partial C_{sh,b,H_2}}{\partial z}\Big|_{z=L} = 0\,;\, \frac{\partial C_{sh,b,H_2}}{\partial r}\Big|_{r=R/2} = \frac{k_{bs}}{D_{r,eff,H_2}}\left(C_{sh,b,H_2} - C_{sh,s,H_2}\right) - \frac{\pi}{L}J_{H_2}\,,\, \frac{\partial C_{sh,b,H_2}}{\partial r}\Big|_{r=0} = 0 \quad (8)$$

2.7 Solid phase's mass transfer in the shell side

As the solid phase can't permeated through Pd-based membrane, all Chemical components (i = CH_4, CO_2, H_2 and CO) are modelled in the solid phase without none mass flow towards the permeation side. Mass balance equations to each component i on the solid phase in the SFBM reformer module's shell side are described as follows.

- Mass balance of each components i on the solid phase in the shell side;

$$\frac{\partial C_{sh,s,i}}{\partial t} = D_{r,eff,s}\frac{1}{r}\frac{\partial}{\partial r}\left(r\frac{\partial C_{sh,s,i}}{\partial r}\right) - u_s\frac{\partial C_{sh,s,i}}{\partial z} - k_{sb,i}\frac{3}{R_p}\frac{\left(1-\varepsilon_b\right)}{\varepsilon_b}\left(C_{sh,b,i} - C_{sh,s,i}\right) + \rho_s\eta_1 \left[-\left(r_{CH_4} + r_{CO_2}\right) + 2\left(r_{CO} + r_{H_2}\right)\right] \tag{9}$$

- Initial and boundary conditions for Equation (9) are defined as;

$$C_{sh,s,i}\Big|_{t=0} = C_{sh,s,i,0}\,;\; C_{sh,s,i}\Big|_{z=0^+} = C_{sh,s,i,in.}\,,\; \frac{\partial C_{sh,s,i}}{\partial z}\Big|_{z=L} = 0\,;\; \frac{\partial C_{sh,s,i}}{\partial r}\Big|_{r=R/2} = \frac{k_{sb}}{D_{r,eff,s}} \tag{10}$$

$$\left(C_{sh,b,i} - C_{sh,s,i}\right),\; \frac{\partial C_{sh,s,i}}{\partial r}\Big|_{r=0} = 0$$

There are complementary equations in Equations (1)-(10). These equations are used to supplement the mathematical model's energy and mass equations and can be found in Equations (11) and (12) below.

$$r_{CH_4} = -R_{CO_2},\; r_{CO_2} = -R_{CO_2},\; r_{H_2} = +2R_{CO_2},\; and\;\; r_{CO} = +2R_{CO}; \tag{11}$$

$$J_{H_2} = \frac{Q_0}{\delta_m}exp\left(-\frac{E_{H_2}}{R_u T_{op.}}\right)\left[\left(P_{H_2}^{sh.}\right)^{0.5} - \left(P_{H_2}^{per.}\right)^{0.5}\right] \tag{12}$$

2.8 Permeate side

The amount of permeated H_2 depends not only of the membrane properties, but it is also a function of the recovery of H_2 in the permeation side. A mass balance equation was developed for the permeation side as follows.

$$L\frac{dY_{H_2}^{per}}{dz} = \frac{2\pi L R_m}{F_{CH_4,0}}J_{H_2}\,;\; F_{H_2}^{per}\Big|_{z=0^+} = 0,\; and\;\; \frac{dY_{H_2}^{per}}{dz}\Big|_{z=L} = 0 \tag{13}$$

From hydrogen recovery $\left(Y_{H_2}^{per}\right)$, it can be computed the concentration of hydrogen on the permeation side as follows.

$$C_{H_2}^{per} = \frac{P_{op}^{per.}}{R_u T_{op}^{per}}Y_{H_2}^{per} \tag{14}$$

2.9 Model equations numerical solution

The numerical solution of the mathematical model was carried out for a numeric method which ensures numerical stability (Cruz and Abreu, 2017). The proposed model was solved by the finite volume method (FVM) in together with prescribed initial and boundary conditions to analyze the performance of the SFBM reformer module.

3. RESULTS AND DISCUSSIONS

The mathematical modelling was used to investigate the performance from SFBM reformer module using the solar energy's thermal energy. The physical parameters used to obtain the results are shown in Table 1 as follows.

Table 1. Physical parameters used to obtain the simulation results.

Parameters	Values
Kinetic constant (k_{CO2}), kmol/ $kg_{cat.}$sec.	$5.775x10^{5}$
Adsorption constant of CH_4 (K_{CH4}), kPa^{-1}	$2.4317x10^{-6}$
Adsorption constant of CO_2 (K_{CO2}), kPa^{-1}	$3.9008x10^{-5}$
Partial pressure (P_{CH4}), kPa	5.5664
Partial pressure (P_{CO2}), kPa	4.8471
Inlet bubble Temperature ($T_{sh,\,b,\,in}$), K	723
Void fraction (ε_b), m^3 gas/m^3 reformer	0.92
Radial bubble thermal cond .($\lambda_{r,eff,b}$), $W\ m^{-1}K^{-1}$ (1)	0.126
Bubble cap. in the shell side ($C_{P,sh,b}$), $kJ\ kg^{-1}K^{-1}$ (1)	0.967
Bubble velocity (u_b), $m\ s^{-1}$	0.721
Bubble density ($\rho_{sh,b}$), $kg\ m^{-3}$	0.0836
Bubble -solid heat transfer coef. (h_{bs}), $W\ m^{-2}s^{-1}$ (1)	45.73
Interphase specific surface area (A_{bs}), m^{-1}	1700
Membrane thickness (δ_W), µm	3.5
Solid density ($\rho_{sh,s}$), $kg\ m^{-3}$	1400
Solid cap. in the shell side ($C_{P,sh,s}$), $kJ\ kg^{-1}K^{-1}$	0.267
Solid thermal conductivity ($\lambda_{r,eff,s}$), W $m^{-1}K^{-1}$	0.371
Radial dispersion coef. of bubble ($D_{r,eff,b}$), m^2s^{-1}	2.5×10^{-5}
Mass transfer coef. of bubble (k_{bs}), $m\ s^{-1}$	1.02×10^{-2}
Radial dispersion coef. of H_2 ($D_{r,eff,H2}$), m^2s^{-1}	3.47×10^{-6}
Radial dispersion coef. of steam ($D_{r,eff,s}$), m^2s^{-1}	5.234×10^{-4}
Radial dispersion coef. of steam ($D_{r,eff,s}$), m^2s^{-1}	5.234×10^{-4}

(1) Computed at 450 °C

3.1 Numerical experiments

Chemical equilibrium is the state in which the forward and backward reaction rates are equal. For this condition, there is no shift in concentrations of the reactants and products. In addition, the thermodynamic equilibrium occurs when a system reaches the chemical and thermal equilibriums. In this study, chemical equilibrium is connected to the mathematical model through the reaction rate's (Eq. (2)) equation. Figure 2 shows the endothermic reaction's temperature profiles in the shell side with particles of β-SiC open-cell foam to three different radial positions.

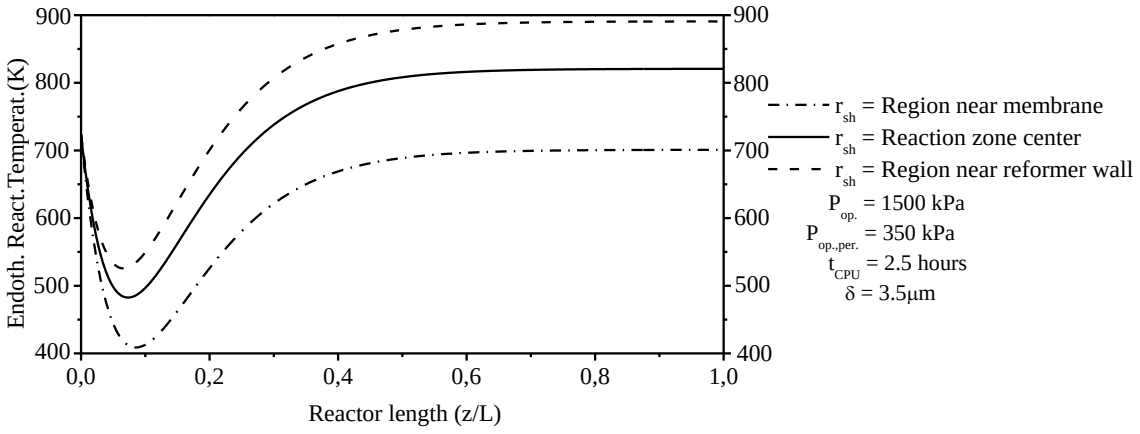

Figure 2. Temperature profiles versus reformer length for three different radial positions to an average effective radial conductivity $\left(\lambda_{r,eff,s} = 0.179\ \mathrm{W}\ m^{-1}K^{-1}\right)$

Because of the endothermic nature of the reforming reaction, heat is supplied into by means of external heating. Therefore, the SFBM reformer' reaction zone and catalyst particles are exposed to significant temperature gradients. Figure 2 describes a significant decrease of the reaction temperature towards to Pd-based membrane due to thermodynamic equilibrium's shift.

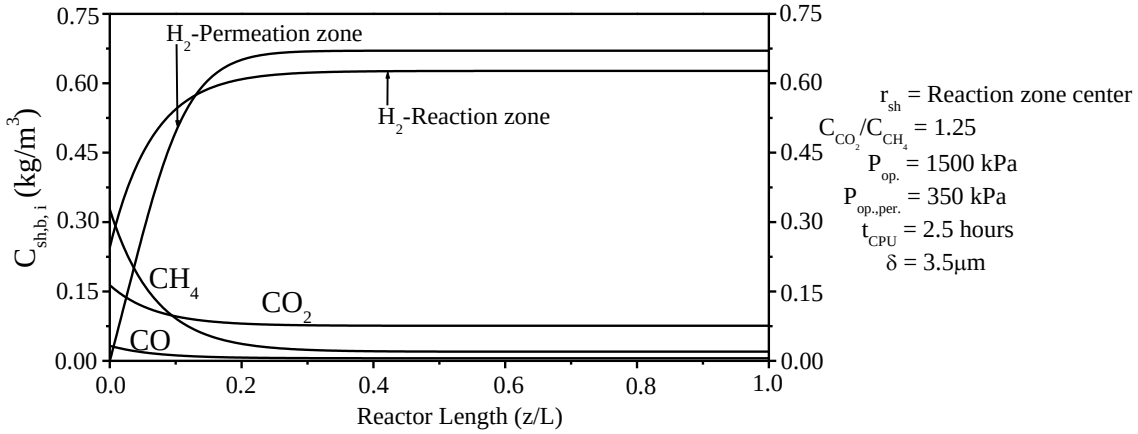

Figure 3. Mole concentration of the components versus reformer length at averaged radial position to an average effective radial conductivity $\left(\lambda_{r,eff,s} = 0.179\ \mathrm{W}\,m^{-1}K^{-1}\right)$

Figure 3 shows that the distribution of the gaseous products can reach to stable levels instantly after introducing the initial values. As it can be observed in Figure 3, the reactant mole concentration (CH_4 and CO_2) distributions decrease sharply along SFBM reformer bed and therefore, reactant mole concentration distributions have small fluctuation along SFBM reformer bed up to the gas outlet surface. The mole concentration of H_2 (reaction and permeation regions) increases remarkably at the near gas inlet surface region and reaches their maximum values at the gas outlet surface.

After reporting the temperature profiles at the radial positions in the shell side, it is possible to compute the conversions of CH_4 and CO_2 at the region near membrane.

$$X_{CH_4} = 1 - \frac{C_{sh,s,CH_4}}{C_{sh,s,CH_4,in}} \tag{15}$$

$$X_{CO_2} = 1 - \frac{C_{sh,s,CO_2}}{C_{sh,s,CO_2,in}} \tag{16}$$

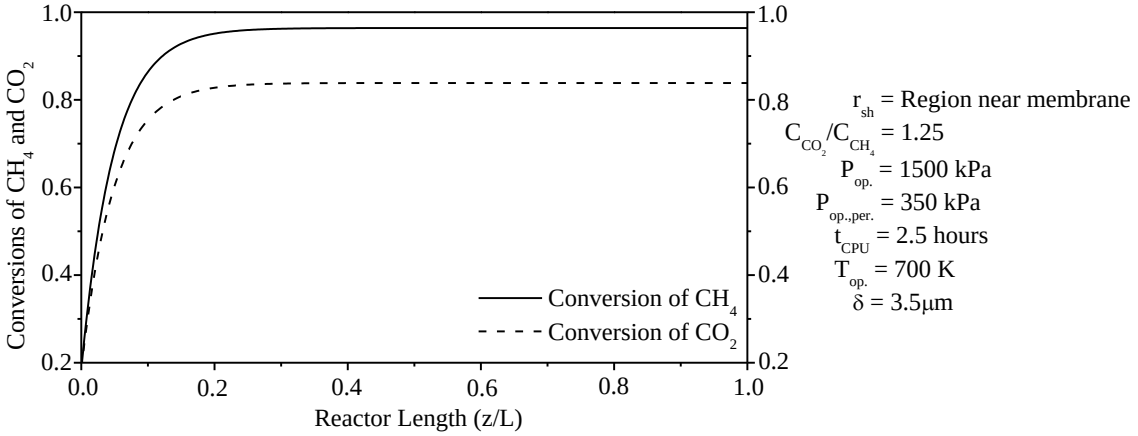

Figure 4. Conversion of CH_4 and CO_2 versus reformer length at near membrane radial position to an average effective radial conductivity $\left(\lambda_{r,eff,s} = 0.179\ \mathrm{W}\,m^{-1}K^{-1}\right)$

The major advantage of dry reforming of CH_4 in membrane reactors is the conversion progress of by the hydrogen removal through the selective membrane, but the conversion of reactants (CH_4 and CO_2) is usually limited by the thermodynamic equilibrium due to equilibrium-limited reversible kinetics rate. Figure 4 reports a comparison between the conversion of CH_4 and conversion of CO_2 along SFBM reformer length.

4. CONCLUSIONS

This work has been focused on the physical-mathematical modelling of the heat and mass transfer for a SFBM reformer module. An analysis to report the performance of the reaction temperature, production of H_2, and conversion of CH_4 and CO_2 is carried out and can be summarized the following conclusions:

1. Pd-based membrane has a significant effect on the thermodynamic equilibrium's shift and thus, the SFBM reformer operates on lower temperature in comparison to a conventional reformer.
2. The amount of H_2 in the permeation zone is higher in comparison with the quantity of H_2 in the reaction zone
3. The overall conversions of reactants have reached the maximum values of 0.9617 (CH_4) and 0.8321 (CO_2).

5. ACKNOWLEDGEMENTS

The authors are grateful to University of Pernambuco for the financial support given (Project 127/2019).

6. REFERENCES

Anjos, E., Damasceno, J., Oliveira, C., Silva, A. and Silva, J., 2018. "Numerical Analysis of the steam reforming of toluene to produce hydrogen in a fixed bed catalytic reactor. In *Proceedings of the 17th Brazilian Congress of Thermal Sciences and Engineering – ENCIT 2018.* Águas de Lindoia - SP, Brazil.

Chein, R. Y., Hsu, W. H. and Yu, C. T., 2017. "Parametric study of catalytic dry reforming of methane for syngas production at elevated pressures". *Int J Hydrogen Energy*, Vol. 42, pp. 14485-14500.

Chen, X., Wang, F., Yan X., Han, Y., Chen Z. and Jie Z., 2018. "Thermochemical performance of solar driven CO_2 reforming of methane in volumetric reactor with gradual foam structure". *Energy*, Vol. 151, pp. 545-555.

Cruz, B. M. and Silva, J. D., 2017. "A two-dimensional mathematical model for the catalytic steam reforming of methane in both conventional fixed-bed and fixed-bed membrane reactors for the Production of hydrogen. *Int J Hydrogen Energy*, Vol. 42, pp. 23670-23690.

Jin, J., Wei, X., Liu, M., Yu, Y., Li, W., Kong, H. and Hao, Y., 2018. "A solar methane reforming reactor design with enhanced efficiency". *Applied Energy*, Vol. 226, pp. 797-807.

Nagy E., 2010. "Coupled effect of the membrane properties and concentration polarization in pervaporation: Unified mass transport model". *Separation and Purification Technology*, Vol. 73, pp. 194-201.

Silva, J. D. and Abreu, C. A. M., 2016. "Modelling and simulation in conventional fixed-bed and fixed-bed membrane reactors for the steam reforming of methane". *Int J Hydrogen Energy*, Vol. 41, pp. 11660-11674.

Villafán-Vidales H. I., Arancibia-Bulnes C. A., Riveros-Rosas D., Romero-Paredes H., Estrada C. A., 2017. "An overview of the solar thermochemical processes for hydrogen and syngas production: Reactors and facilities". *Ren Sust Energy Reviews*, Vol. 75, pp. 894-908.

7. RESPONSIBILITY NOTICE

The author(s) is (are) the only responsible for the printed material included in this paper.